Journal of
Ceramic Science
and Technology

J. Ceram. Sci. Tech., **08** [01] 161-168 (2017)
DOI: 10.4416/JCST2016-00105
available online at: http://www.ceramic-science.com

Relationship of Optical Properties and Elastoplastic Characteristics of Transparent Spark-Plasma-Sintered YSZ Ceramics

O. L. Khasanov*, E. S. Dvilis, Z. G. Bikbaeva, V. D. Paygin, A. O. Khasanov

Department of Nanomaterials and Nanotechnologies, National Research
Tomsk Polytechnic University, Tomsk, Russia-634050

received October 31, 2016; received in revised form December 31, 2016; accepted January 21, 2017

Abstract

Transparent yttria-stabilized zirconia (YSZ) ceramics were sintered with the SPS method in different conditions. The optical and corresponding mechanical properties of the sintered samples were studied. A parameter for optimizing SPS processing has been suggested which characterizes optical transparency versus sample thickness. The dynamic evolution of the swelling areas over time after local indentation of transparent YSZ ceramics was shown. The appearance of spalls from the swelling areas depends on the degree of internal mechanical stresses in the given region of the sample and is explained by the relaxation of stresses accumulated on deformation during static indentation.

Keywords: YSZ, transparent ceramics, optical properties, mechanical properties, indentation, swelling, spalls, stress relaxation dynamics

I. Introduction

Yttria-stabilized zirconia (YSZ) ceramics exhibit a unique combination of mechanical and optical properties including high values of fracture toughness, refractive index, oxygen diffusivity and low thermal conductivity [1,2]. Therefore, studies of transparent YSZ ceramics having tetragonal or cubic crystalline structure are of immediate interest. The presence of oxygen vacancies in this material allows a shift in the spectrum of light transmission in the IR region, which makes such ceramics promising for application as IR windows [3].

For the manufacture of transparent ceramics, including YSZ, the SPS method (spark plasma sintering, or pulsed electric current sintering) is used, as this allows the production of ceramics with good optical properties [1,3–9].

Lei *et al.* [4] showed that optical transparent YSZ-ceramics may be obtained with the SPS method at a temperature of 1300 °C and compacting pressure of 50 MPa. H.B. Zhang *et al.* sintered transparent YSZ ceramics with the SPS method at a higher pressure of 400 MPa and sintering temperature of 1050 – 1200 °C [5,6]. Garay *et al.* [7,8] obtained transparent YSZ ceramics with the SPS method and 2-stage compaction (under 106 MPa and then under 141 MPa). The relationship between the thermal conductivity and grain size of transparent YSZ ceramics manufactured with the SPS method is analyzed in the work [9].

In contrast with other optical transparent ceramic materials (Al_2O_3, $MgAl_2O_4$, YAG, Y_2O_3), changes in the elastoplastic properties of transparent YSZ ceramics in relation with optical properties have not been studied sufficiently. Garay *et al.* [7,8] defined the fracture toughness for transparent 8YSZ ceramics (cubic structure of zirconia)as 3.1 MPa·m$^{1/2}$, that is higher than the value of fracture toughness of sapphire single crystal (1.2 MPa·m$^{1/2}$) and polycrystalline Al_2O_3 (1.8 MPa·m$^{1/2}$). It is noted that the mechanical properties (hardness and toughness) of optical transparent YSZ ceramics are sensitive to the concentration of grain boundaries. Anselmi-Tamburini *et al.* [10] estimated the hardness of cubic zirconium ceramics as 13.3 GPa, this value is 3 % lower than that of one of its single crystals. The Young's modulus for opaque 8YSZ ceramics was defined by Lakki *et al.* [11], its value is 200 GPa, that is close to the Young's modulus of YSZ single crystal (233 GPa [12]). Optical and corresponding mechanical properties of transparent YSZ ceramics were presented by Tsukuma *et al.* [2]: the ceramics had a Young's modulus of 200 GPa, fracture toughness was 1.8 MPa·m$^{1/2}$, and the hardness measured according to the Vickers method was 11.76 GPa at in-line transmission 74 %.

A negligible influence of the grain size of nanocrystalline, opaque 8YSZ ceramics sintered with various methods (SPS, hot pressing, conventional sintering) on their microhardness (12.5 – 13.5 GPa) and fracture toughness (1.5 – 1.3 MPa·m$^{1/2}$) was shown by Dahl *et al.* [13]. Elastoplastic properties of partially stabilized zirconia 2Y-TZP (tetragonal crystalline structure) were studied in [14] and in [15–18] for translucent dental 3Y-TZP.

However, the named works only state values of elastoplastic parameters with optical properties that correspond to these samples. The behavior of transparent YSZ ceramic under local loading (indentation) and the aftereffect after unloading remain unstudied.

In this connection, the present work is devoted to the study of the relationship of the optical properties of transparent YSZ ceramics with its elastoplastic characteristics as well as dynamics of its deformation and failure after local static loading (indentation).

* Corresponding author: khasanov@tpu.ru

II. Experimental Procedure

For the study, we used commercially available granulated cubic zirconia (ZrO_2) nanopowder stabilized with 10 mol% Y_2O_3 (TZ-10Y, Tosoh Corp.). The purity of the powder was 99.9 %, the average particle size was 90 nm, the specific surface area was 6 ± 2 m^2/g.

The powder was consolidated with the SPS method using an SPS-515S installation (Syntex Inc.). The sintering conditions of the YSZ ceramics are presented in Table 1.

Table 1: SPS conditions for YSZ ceramics samples.

Sample №	Sintering temperature, (°C)	Heating rate, (°C/min)	Dwell time at max. temperature, (min)	Compaction pressure, (MPa)
Cer1	1300	10	10	72
Cer2	1400	93	10	72
Cer3	1300	93	10	72
Cer4-ox	1300	10	10	72

Sample Cer4-ox was annealed in air at a temperature of 1000 °C for 2 h for partial saturation of oxygen vacancies.

The optical characteristics of the sintered ceramics were measured with a double-beam UV-1800 spectrophotometer (Shimadzu).

The elastic and plastic characteristics and microhardness of sintered YSZ-ceramics were studied based on the method of indentation with the Vickers pyramid in "loading-unloading" mode with a DUH-211S dynamic ultramicro hardness tester (Shimadzu) at a load of 1.96 N.

Measurements of the microhardness were performed with a PMT-3M (LOMO) microhardness tester at a load of 1.96 N using the standard method of indentation with the Vickers pyramid. Fracture toughness was measured with the same installation under a load of 4.9 N.

All measurements of the elastoplastic characteristics of the samples were performed after these had been polished.

The coefficient of fracture toughness K_{1c} is calculated on the basis of measurement of the lengths of the radial cracks forming under indentation according to Niihara's formula [19]:

$$K_{1C}=0{,}035\frac{H_v a^{\frac{1}{2}}}{\Phi}\left(\frac{l}{a}\right)^{-\frac{1}{2}}\left(\frac{H_v}{E\Phi}\right)^{-\frac{2}{5}} \qquad (1)$$

Here H_V is the hardness; E is the Young's modulus; a is the Vickers indent half-diagonal; l is the length of the radial (Palmqvist) crack from the Vickers indent; $0.25 \le l/a \le 2.5$ for Palmqvist cracks; Φ is the constraint factor (≈ 3).

Lateral cracks in transparent materials forming below the sample surface and propagating outward from edges of the Vickers pyramid are fixed with an optical microscope in the form of light segments – "petals", the area of which can be measured. Changes of these areas in the time were fixed in the periods from 1 min to 72 h using an optical microscope and a VEC-335 digital camera.

The topology of areas of local failure on the samples' surfaces around the indent (under indentation loads of 49 – 98.1 N) was studied using a Micromeasure 3D Station (STIL) profilometer.

The geometric parameters of the failure on the obtained images were calculated using "Image J" software.

III. Results and Discussion

(1) Optical properties

The main part of the light transmission spectrum of the studied samples is within the short-wave region of infrared wavelength range ($\lambda > 1$ μm, Fig. 1). The optical characteristics of ceramics obtained at various temperatures differed from each other. In-line transmission of sample Cer3, sintered at temperature of 1300 °C was 24.5 % greater than that of sample Cer2 (the sintering temperature was 1400 °C), and the optical density is 0.6 less. Such a significant difference in the optical properties can be explained with the fact that increasing sintering temperature leads to increasing concentration of oxygen vacancies, and, as a result, the transmission spectrum is displaced in the IR region. These results are consistent with the work [5] in which the authors found that light transmittance of YSZ-ceramics depends significantly on the sintering temperature.

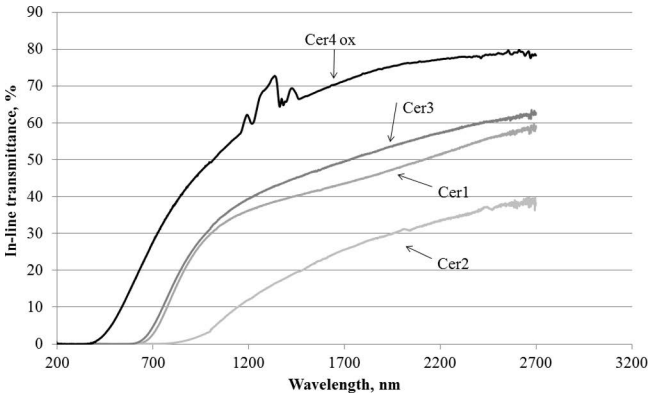

Fig. 1: Spectra of the light transmittance for the studied YSZ ceramics samples.

Fig. 1 shows that subsequent annealing in an oxygen-containing atmosphere improves the optical properties of YSZ ceramics owing to filling of the oxygen vacancies in the structure of YSZ as a result of oxygen diffusion [5, 6]. Therefore, in-line transmission of sample Cer4-ox in the middle of the visible range (λ = 555 nm) after the thermal annealing in air increased to 11.9 %, and in infrared range (λ = 1620 nm) increased to 69.7 %.

Table 2 shows the values of the optical properties of researched samples.

The analysis showed that optical properties of the studied ceramics can be described with Eq. (2), which relates the optical density D of the ceramics for the given wavelength λ with sample thickness h:

$$\frac{D}{h}=\frac{1}{k\cdot\ln\left(\frac{\lambda}{\lambda_0}\right)+h_{0.1}} \qquad (2)$$

where λ is the current wavelength of radiant flux through the sample, $\lambda_0 = 740$ nm is the wavelength of the left edge of IR-range, k is the rate of decreasing optical density versus λ_0 increase, $h_{0.1}$ is the sample thickness at which the radiant flux having $\lambda_0 = 740$ nm will attenuate ten times.

Table 2: Optical properties of YSZ ceramics samples.

Sample	In-line transmittance at λ=555 nm (%)	In-line transmittance at λ=1620 nm, (%)	Optical density D per 1 mm thickness at λ=1100 nm (mm^{-1})	Optical quality, (mm/nm)
Cer1	0	42.48 [±0.13]	0.36 [±0.01]	4.06
Cer2	0.10 [±0.01]	23.79 [±0.07]	0.93 [±0.01]	0.67
Cer3	0.02 [±0.01]	48.26 [±0.14]	0.33 [±0.01]	5.09
Cer4-ox	11.91 [±0.03]	69.76 [±0.20]	0.15 [±0.01]	24.5

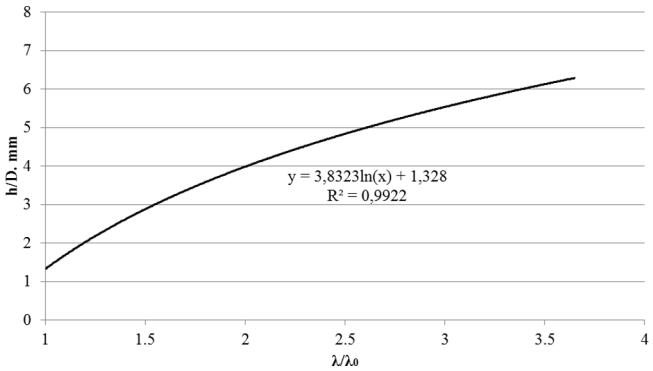

Fig. 2: Ratio of the YSZ sample thickness h and optical density D vs wavelength of radiant flux λ through the sample.

Fig. 2 presents the obtained dependence of the thickness h and optical density D of the YSZ sample on the wavelength of the radiant flux λ through the sample.

Obviously, the maximum values of coefficients k, $h_{0.1}$ characterize the ceramics samples with the best optical properties. The product $(k \cdot h_{0.1})$ has the highest value for the samples with the best optical properties (Cer4-ox – the annealed sample and Cer3 of the non-annealed samples) – Table 2, that does not correlate directly with the SPS conditions – Table 1. Therefore, a complex parameter $(k \cdot h_{0.1})$ can be regarded as the parameter of "optical quality" and can be used to optimize SPS modes of transparent ceramics.

(2) Mechanical properties

As a characteristic of the scale of change of the sample surface relief around the indents after indentation with the diamond Vickers pyramid we used the total area of the four segments around each indent that have shape of "petals" as a result of the swelling surface (Fig. 3):

$$S = S_A + S_B + S_C + S_D \quad (3)$$

Areas S_i were measured using the "Image J" code. It was shown experimentally that after indentation the total area S increases with time t according to logarithmic law (Fig. 4):

$$S(t) = v_1 \cdot \ln t + S_1 \quad (4)$$

where v_1 is the instant growth rate of the swelling area within 1 minute after indentation time t_0 (the constant); S_1 is the total area of swelling within 1 minute after indentation (the constant).

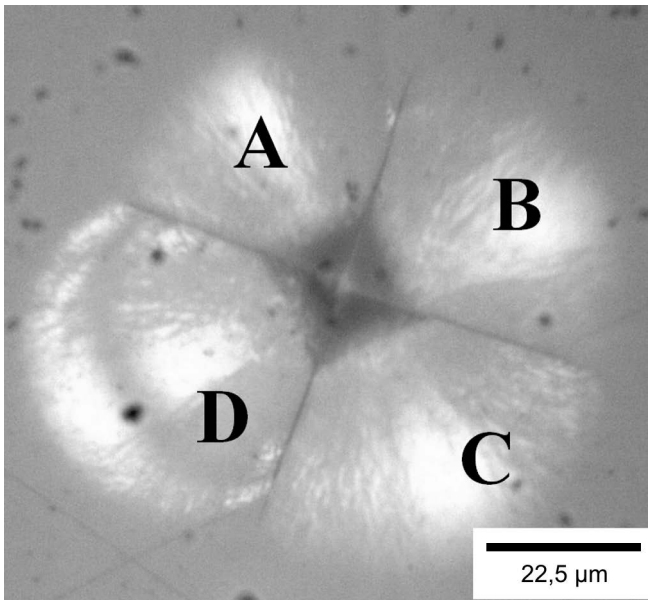

Fig. 3: Designation of the areas with lateral cracks under the sample surface around the indent (the Cer3 sample).

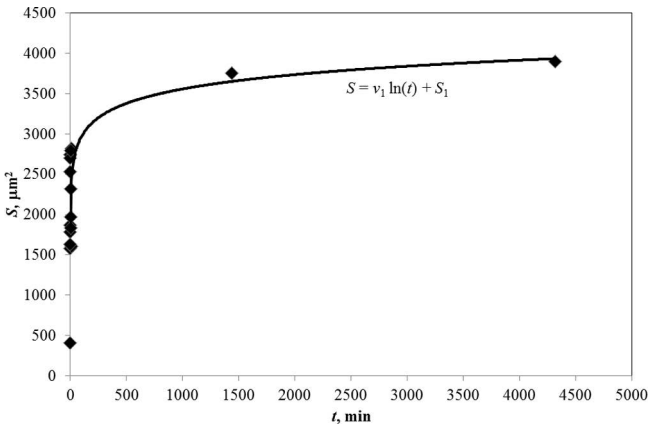

Fig. 4: Total area of the failure regions around the indent vs time after indentation.

Determination of coefficients v_1 and S_1 of Eq. (4) for the studied samples of transparent YSZ ceramic allows qualitative estimation of the dynamics of their surface failure. Such local failure is explained with the relaxation of stresses, accumulated upon deformation in the process of static indentation.

Table 3: Mechanical properties of the transparent YSZ ceramics.

Sample	Young modulus, (GPa)	Micro-hardness, (GPa)	Fracture toughness, (MPa·m$^{1/2}$)	Growth rate of swelling area v_1, (μm^2/min)	Total swelling area S_1, (μm^2)	Optical quality $(k \cdot h_{0.1})$, (mm/nm)
Cer1	107.5 [±1.6]	14.24 [±0.21]	3.08 [±0.04]	285.6	3216	4.06
Cer2	103.0 [±1.5]	14.02 [±0.21]	3.05 [±0.04]	305.7	1826	0.67
Cer3	107.9 [±1.6]	14.37 [±0.21]	3.11 [±0.04]	259.3	1854	5.09
Cer4-ox	170.7 [±2.6]	13.95 [±0.20]	2.23 [±0.03]	-	2416	24.5

Parameters v_1 and S_1, as well as the corresponding values of Young's modulus, microhardness, fracture toughness, and the complex parameter $(k \cdot h_{0.1})$ for the studied samples, are presented in Table 3.

Fig. 5 shows the dependences of the instant growth rate of the swelling area v_1 for non-annealed YSZ samples versus creep at the indentation (Fig. 5a), microhardness (Fig. 5b), fracture toughness (Fig. 5c), and complex parameter $(k \cdot h_{0.1})$ (Fig. 5d).

Monotonic correlation of behavior v_1 is observed with the elastoplastic characteristics of non-annealed samples: creep at indentation C_{it}, microhardness H_V, fracture toughness K_{Ic} as well as with complex parameter of optical quality $(k \cdot h_{0.1})$.

The dependences presented in Fig. 5 reflect processes of relaxation of mechanical stresses accumulated upon local surface deformation of transparent YSZ ceramics in the indentation process and demonstrate the correlation of the elastoplastic properties of the ceramics with the complex parameter of optical quality $(k \cdot h_{0.1})$.

The formation of swelling regions and their subsequent spalling after indentation of the samples were observed experimentally, and this process evolved with time.

Images of spalling around the indents in the studied YSZ samples with time after indentation are presented in Figs. 6 – 8.

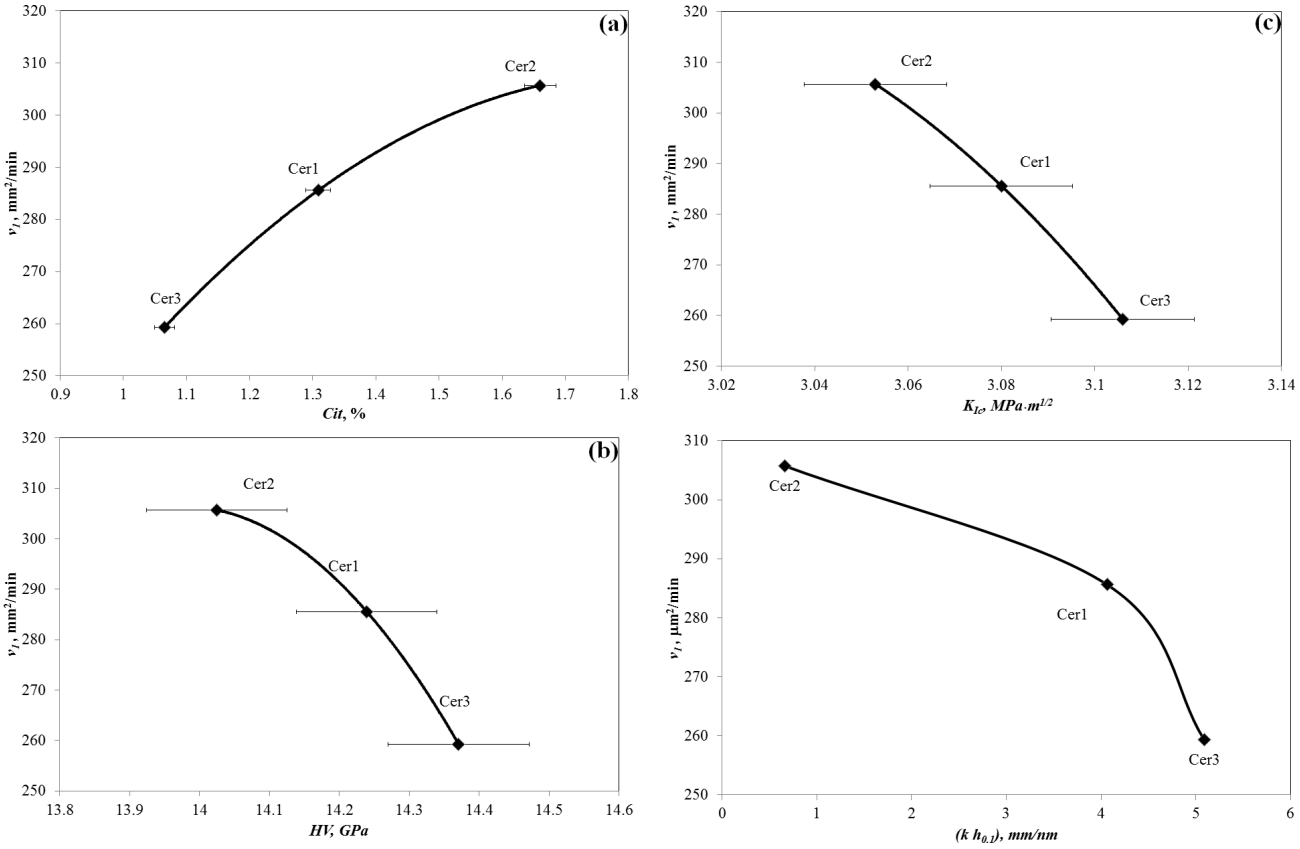

Fig. 5: Correlations of the instant growth rate of the swelling area v_1 with creep at indentation (a), microhardness (b), fracture toughness (c) and parameter of optical quality ($k \cdot h_{0.1}$) (d) for the non-annealed YSZ samples.

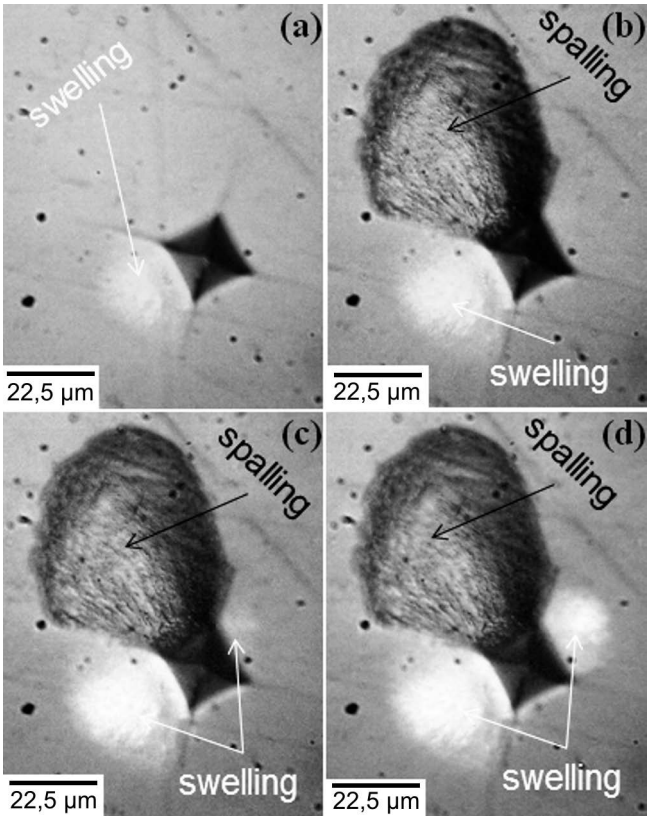

Fig. 6: Evolution of the local failure areas around the indent in the Cer3 sample with time after indentation: (a) in 1 minute after indentation, (b) in 2 minutes, (c) in 3 minutes, (d) in 5 minutes after indentation. Indentation load 4.9 N.

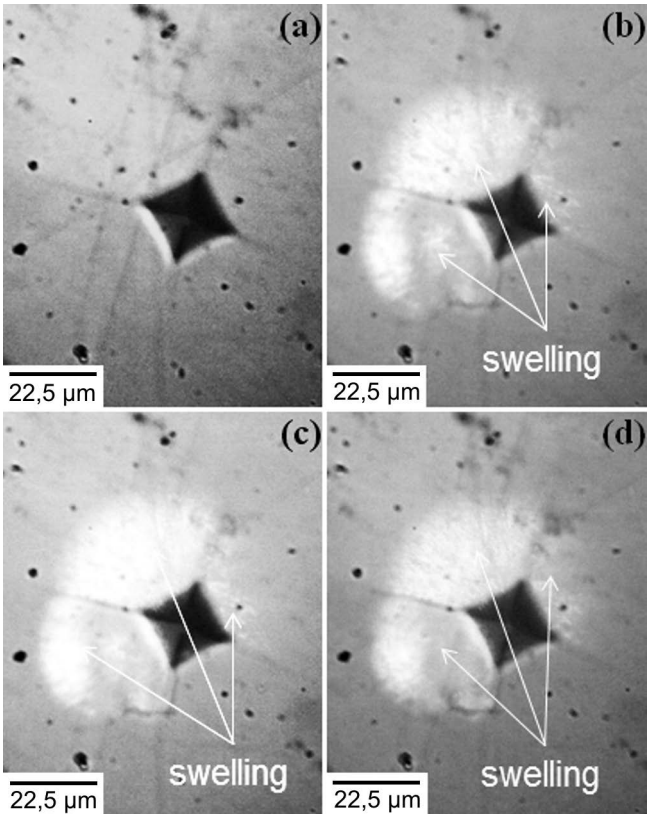

Fig. 7: Evolution of the local failure areas around another indent in the Cer3 sample with time after indentation: (a) in 1 minute after indentation, (b) in 2 minutes, (c) in 3 minutes, (d) in 6 minutes after indentation. The spalls were not observed. Indentation load 4.9 N.

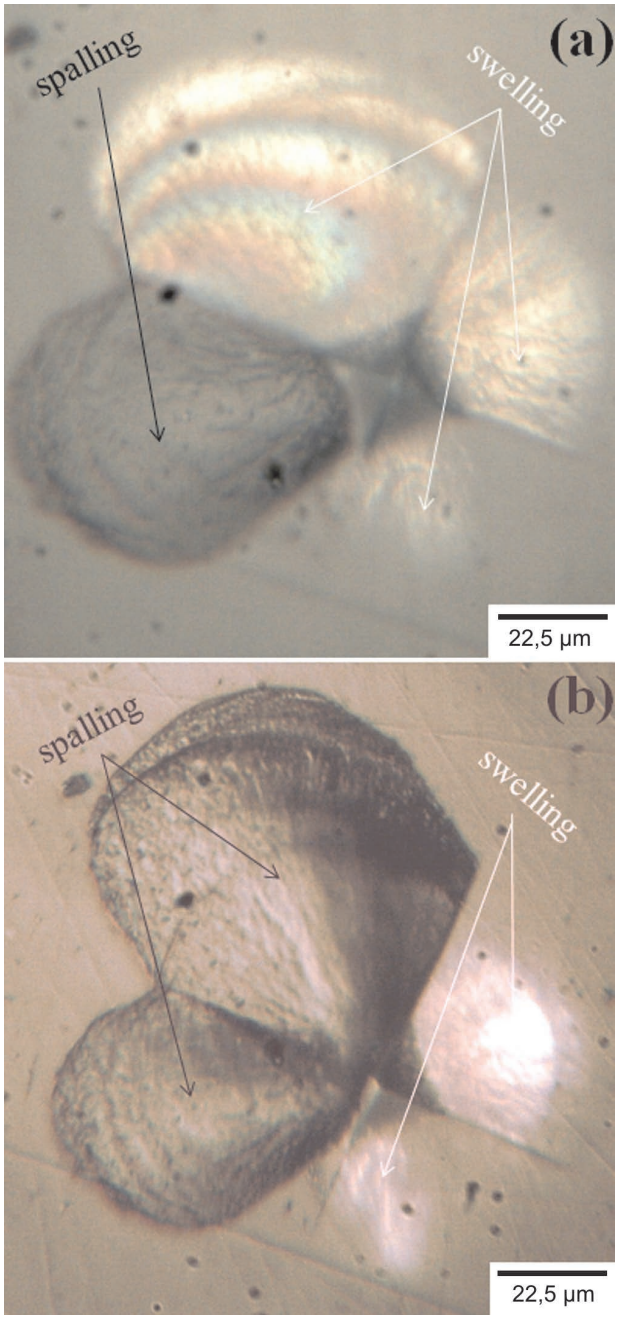

Fig. 8: Evolution of the local failure areas around the indent in the Cer1 sample with time after indentation: (a) in 1 minute after indentation, (b) in 24 hours after indentation. Indentation load 4.9 N.

Growth of local failure areas around the indent with time is explained as follows. Under loading by the indenter, radial cracks propagating from the indent angle are formed first. As the load increases, the average length of the cracks increases, and median cracks are formed between the radial cracks. The latter also grow and intersect the radial cracks forming a crack network in a shape close to half-disks ("petals") in the segments adjacent to indent edges. Then, a series of sub-surface cracks appears, which are located between radial ones and propagate parallel to surface, which is observed as swelling of the segment. The duration of the growth of the swelling area may vary from a few minutes to several hours – depending on the degree of internal mechanical stresses in this sample region.

After unloading, high tensile stresses appear around the deformed zone and lead to crack growth up to the surface. Relaxation of accumulated local stresses may lead to spalling of any segment.

Similar patterns of aftereffect at the indentation were observed by Nosov *et al.* [20] for corundum single crystals and they noted that the spalling process has a probabilistic nature: spalling has been observed only in 15 – 20 % of studied indents.

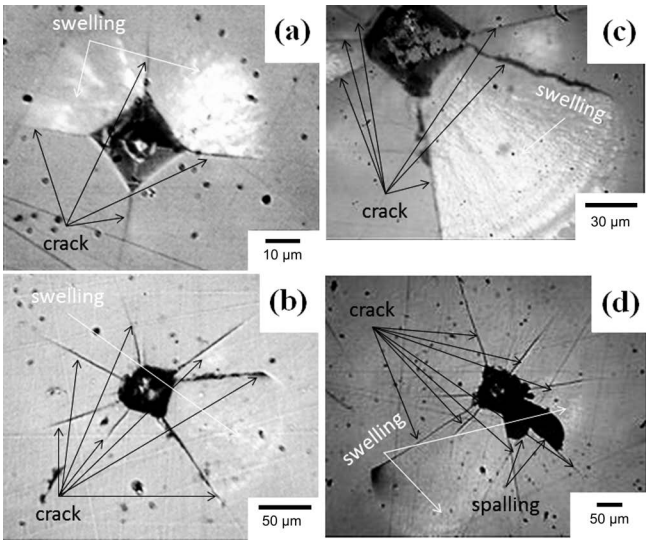

Fig. 9: Local failure areas around the indent in the Cer2 sample at different indentation loads: (a) 4.9 N, (b) 98.1 N, (c) 49 N, (d) magnified image of the indent (c).

Time from unloading until spalling of the segments in the studied samples of YSZ ceramics can last from several minutes to tens of hours. For example, for the Cer1 sample this period lasts about 24 hours (Fig. 8).

The white color of swelling areas around the indents is explained with effects of light transmission through subsurface crack networks in transparent YSZ ceramics. Since the depth of the swelling segment varies from the indent edge to the segment periphery, on illumination an interference pattern is observed that reflects the formation of subsurface lateral cracks [21].

Fig. 9 shows failure areas of the Cer2 sample surface under different indention loads: 4.9 N, 49 N and 98.1 N. Under the highest load, spalling of one segment was observed (Fig. 9-b).

The results of surface profilometry of the relief of the YSZ ceramic samples in the vicinity of the indent are presented in Figs. 10 a, b, c. Scanning of the ceramics surface was started from the point out of the failure area ("0"), passed through the indent and/or through the swelling region – up to the undestroyed area (point "l"). The profilograms reflect the height of the swelling regions, and the crack depth in the studied areas of the YSZ ceramics.

Thus, it was shown that indentation of optically transparent samples of YSZ ceramics leads to formation of complex patterns of deformation and failure of the surface in the vicinity of the indents that are changed with time after unloading. Formation of spalls from the swelling area has a probabilistic nature, it depends on the degree of internal mechanical stresses in the given sample region, and is explained by the relaxation of stresses accumulated upon deformation in the process of static indentation.

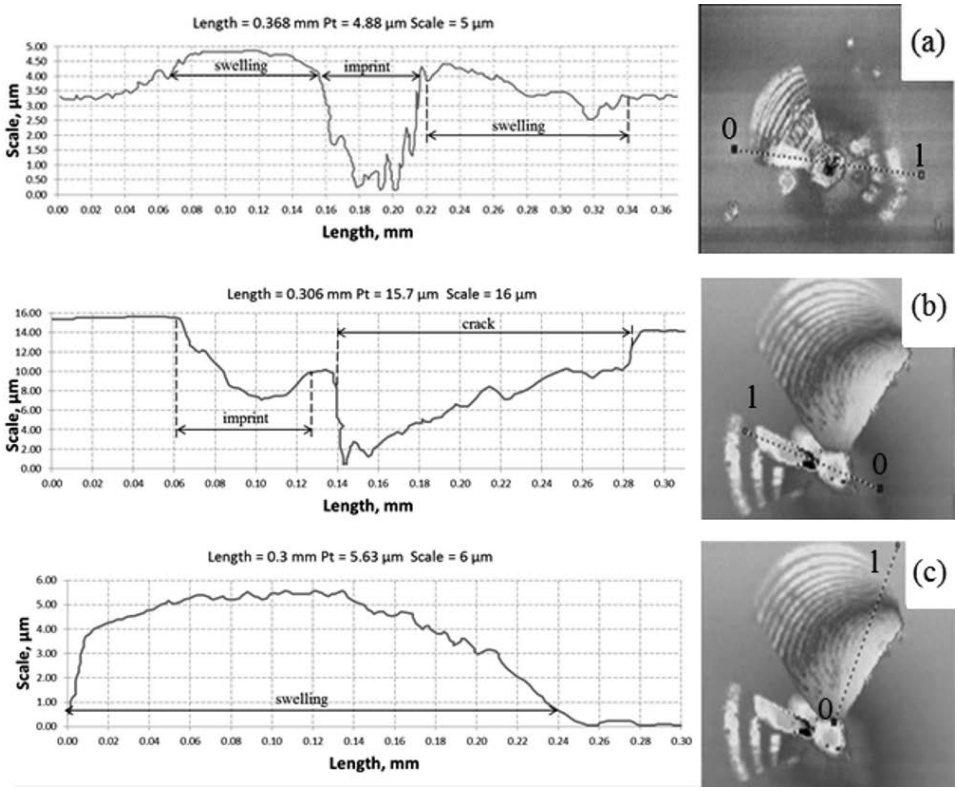

Fig. 10: Profilograms of the surfaces around indents in YSZ ceramics at different indentation loads: a) 49 N; (b), (c) 98.1 N. Along the x-axis - length of the scanned region in mm; along the y-axis -height of the failure profile in μm.

IV. Conclusions

1. Transparent YSZ ceramics were produced by means of spark plasma sintering and showed in-line transmittance up to 12 % in the visible range (λ = 555 nm) and around 70 % in the middle IR-range (λ = 1620 nm).
2. A parameter for optimization of the SPS processing has been suggested which characterizes optical transparency vs sample thickness. This parameter correlates both with optical and mechanical properties of transparent ceramics.
   It is the product of constant coefficients ($k \cdot h_{0.1}$) - rate of decreasing the optical density versus λ increase, and sample thickness at which the radiant flux will attenuate tenfold. This parameter has no direct correlation with the SPS modes, but its maximum value characterizes the best optical and mechanical properties of transparent YSZ ceramics. Thus, it is necessary to choose such modes of SPS process (temperature, pressure, their rate) for manufacturing optical transparent YSZ ceramics wherein said optimization parameter takes the maximum value.
3. Transparent YSZ ceramics after local indentation showed the dynamic evolution of the swelling areas with time, which reflects the dynamics of the local surface failure caused by the relaxation of stresses after indentation.
4. The appearance of spalls from swelling areas has a probabilistic nature, depending on the degree of internal mechanical stresses in a given sample region, and is explained by relaxation of stresses accumulated upon deformation in the process of static indentation.
5. Better optical properties are exhibited by YSZ samples with higher microhardness and fracture toughness, lower creep and slow relaxation of stresses after local indentation (lower instant growth rate of the swelling area). This correlation is observed for non-annealed samples having oxygen vacancies.

References

1 Wang, S.F., Zhang, J., Luo, D.W., Gu, F., Tang, D.Y., Dong, Z.L., Tan, G.E.B., Que, W.X., Zhang, T.S., Li, S., Kong, L.B.: Transparent ceramics: Processing, materials and applications, *Prog. Solid State Chem.*, **41**, 20 – 54, (2013).

2 Yamashita, I., Kudo, M., Tsukuma, K.: Development of highly transparent zirconia ceramics, *Tosoh Res. Technol. Rev.*, **56**, 11 – 16, (2012).

3 Zhang, H., Li, Z., Kim, B.-N., Morita, K., Yoshida, H., Hiraga, K., Sakka, Y.: Highly infrared transparent nanometric tetragonal zirconia prepared by high-pressure spark plasma sintering, *J. Am. Ceram. Soc.*, **94**, [9], 2739 – 2741, (2011).

4 Lei, L.W., Fu, Z.Y., Wang, H., Lee, S.W., Niihara, K.: Transparent yttria stabilized zirconia from glycine-nitrate process by spark plasma sintering, *Ceram. Int.*, **38**, [1], 23 – 28, (2012).

5 Zhang, H.B, Kim, B.-N., Morita, K., Yoshida, H., Lim, J.-H., Hiraga, K.: Optimization of high-pressure sintering of transparent zirconia with nano-sized grains, *J. Alloy. Compd.*, **508**, 196 – 199, (2010).

6 Zhang, H.B., Kim, B.-N., Morita, K., Hiraga, H.Y.K., Sakka, Y.: Effect of sintering temperature on optical properties and microstructure of translucent zirconia prepared by high pressure spark plasma sintering, *Sci. Tech. Adv. Mater.*, **12**, 1 – 6, (2011).

7 Alaniz, J.E., Perez-Gutierrez, F.G., Aguilar, G., Garay, J.E.: Optical properties of transparent nanocrystalline yttria stabilized zirconia, *Opt. Mater.*, **32**, 62 – 68, (2009).

8 Casolco, S.R., Xu, J., Garay, J.E.: Transparent/translucent polycrystalline nanostructured yttria stabilized zirconia with varying colors, *Scripta. Mater.*, **58**, 516 – 519, (2008).

9 Ghosh, S., Garay, J.E. *et al.*: Thermal properties of the optically transparent pore-free nanostructured yttria-stabilized zirconia, *J. Appl. Phys.*, **106**, [113507], 1 – 4, (2009).

10 Anselmi-Tamburini, U., Woolman, J.N., Munir, Z.A.: Transparent nanometric cubic and tetragonal zirconia obtained by high-pressure pulsed electric current sintering., *Adv. Funct. Mater.*, **17**, [16], 3267 – 3273, (2007).

11 Lakki, A., Herzog, R., Weller, M. *et al.*: Mechanical loss, creep, diffusion and ionic conductivity of ZrO_2-8 mol% Y_2O_3 polycrystals, *J. Eur. Ceram. Soc.*, **20**, 285 – 296, (2000).

12 Kandil, H.M., Greiner, J.D., Smith, J.F.: Single-crystal elastic constants of yttria-stabilized zirconia in the range 20±700, *J. Am. Ceram. Soc.*, **67**, 341 – 346, (1984).

13 Dahl, P., Kaus, I., Johnsson, M. *et al.*: Densification and properties of zirconia prepared by three different sintering techniques, *Ceram. Int.*, **33**, 1603 – 1610, (2007).

14 Xue, W., Xie, Z., Yi, J., Wang, C.-A.: Spark plasma sintering and characterization of 2Y-TZP ceramics, *Ceram. Int.*, **41**, 4829 – 4835, (2015)

15 Zhang, F., Wanmeensel, K., Batuk, M. *et al.*: Highly-translucent, strong and aging-resistant 3Y-TZP ceramics for dental restoration by grain boundary segregation, *Acta Biomater.*, **16**, 215 – 222, (2015).

16 Ebeid, K., Wille, S., Hamady, A. *et al.*: Effect of changes in sintering parameters on monolithic translucent zirconia, *Dent. Mater.*, **30**, 4419 – 4424, (2014).

17 Zhang, Y.: Making yttria-stabilized tetragonal zirconia translucent, *Dent. Mater.*, **30**, 1195 – 1203, (2014).

18 Hallmann, L., Ulmer, P., Wille, S. *et al.*: Effect of surface treatments on the properties and morphological change of dental zirconia, *J. Prosthet. Dent.*, **115**, 341 – 349, (2016).

19 Niihara, K., Morena, R. Hasselman, D.P.H.: Evaluation of K_{Ic} of brittle solids by the indentation method with low crack-to-indent ratios, *J. Mater. Sci. Lett.*, **1**, 13 – 16, (1982)

20 Nosov, Yu.G., Derkachenko, L.I.: Aftereffect in microhardness testing of corundum, *Tech. Phys.*, 48, [10], 1354 – 1457, (2003).

21 Khasanov, O.L., Struts, V.K., Dvilis, E.S., Bikbaeva, Z.G. *et al.*: Spall fracture of ceramics surface by indentation (In Russian), *Rus. Phys. J.*, **5**, [2], 276 – 282, (2012).